Submitted to Nuclear Physics B

UCRL-18417 Rev.
Preprint

SINGLE-PION PRODUCTION IN K^+p INTERACTIONS AT 4.6 GeV/c

C. Fu, J. MacNaughton, and G. H. Trilling

October 30, 1970

AEC Contract No. W-7405-eng-48

LAWRENCE RADIATION LABORATORY
UNIVERSITY of CALIFORNIA BERKELEY

UCRL-18417 Rev.

DISCLAIMER

UCRL-18417 Rev.

SINGLE-PION PRODUCTION IN K^+p INTERACTIONS AT 4.6 GeV/c[‡]

C. Fu,[‡‡] J. MacNaughton and G. H. Trilling

Department of Physics and Lawrence Radiation Laboratory
University of California, Berkeley, California 94720

October 30, 1970

Abstract: A study of K^+p interactions at 4.6 GeV/c leading to single-pion production is presented. Cross sections for the final states $K\Delta$, $K^*(891)p$, $K^*(1420)p$ are given. Comparison of the results of this study with published K^-p and K^-n data at the same momentum indicates that corresponding K^- cross sections are significantly smaller, but other features such as momentum transfer distributions and density matrix elements are very similar.

1. INTRODUCTION

The interactions of K^+ mesons with nucleons do not exhibit significant s-channel resonance behavior, and have therefore been largely described in terms of t-channel exchange diagrams. Consequently the production characteristics of various two-body or quasi-two-body final states appear to change only slowly and smoothly with incident momentum. One can therefore hope that with data spanning a sufficiently large range of incident momenta an improved understanding of t-channel exchanges may be reached.

In this paper we present data on quasi-two-body final states found in single-pion production in K^+p interactions at an incident momentum of 4.6 GeV/c, and compare our results with those of similar studies at other momenta and with data from corresponding K^-N processes. A preliminary discussion of these data has been given by C. Fu [1].

---

‡ Work supported by the U. S. Atomic Energy Commission.

‡‡Now at: Department of Physics, Illinois Institute of Technology, Chicago, Illinois 60616.

2. EXPERIMENTAL PROCEDURE

The experiment was carried out in the Brookhaven National Laboratory 80-inch hydrogen bubble chamber exposed to a 4.6-GeV/c electrostatically separated K^+ beam at the AGS. The results reported in this paper come from the analysis of the following topologies:

(i) two prong,

(ii) two prong with vee,

(iii) three prong (τ decay).

The reactions studied are the following:

$$K^+ + p \rightarrow K^o + p + \pi^+ \quad (1)$$

$$\rightarrow K^+ + p + \pi^o \quad (2)$$

$$\rightarrow K^+ + n + \pi^+ \quad (3)$$

and $$K^+ \rightarrow \pi^+ + \pi^+ + \pi^- \ . \quad (4)$$

The first measurements of topologies (ii), (iii), and the first two measurements of topology (i) were carried out with the Lawrence Radiation Laboratory Flying-Spot Digitizer (FSD). Further remeasurements were made on Franckenstein measuring projectors. The geometric reconstruction and kinematic fitting were done by the PACKAGE program. The elastic scatters have been discussed elsewhere [2] and will not be considered here. Relevant to this paper, besides the τ decays, are 1C fits of topology (i) and 4C fits of topology (ii). The 1C fits were inspected on the scan table to obtain ionization information. Unfortunately, even after such inspection, considerable numbers of ambiguities remained. In table 1, we give the numbers of events in topologies (i) and (ii) which fit the various single-pion production channels, indicating also how many ambiguous events occurred in each topology. Since these ambiguous events may appear in several different reactions, the total number of 1C fits is less than the sum of the various 1C fits, ambiguous or unambiguous, listed in table 1.

The two-prong-plus-vee and two-prong events were handled separately and do not correspond to quite the same incident beam track length. From normalization with τ decays, the two-prong-plus-vee sample corresponds to an incident flux of 0.77 μb/event. On the other hand the two-prong sample (whose normalization is discussed in ref. 2) corresponds to a flux of 0.83 μb/event.

It is important to note that because of the background of multi-neutral events, not all of the 1C fits correspond to real one-pion production events. Rough estimates indicate that as much as 30% could be multi-neutral background although the actual background is probably rather less. In our subsequent analysis we shall be strictly concerned with the production of clear-cut resonances; with appropriate mass selections nearly pure samples of the desired types of events are obtained.

3. RESULTS

3.1. Cross Sections for KNπ Final States

The $K^{o}p\pi^{+}$ cross section was determined from the 482 events in which the $K_1^o \rightarrow \pi^+\pi^-$ decay [topology (ii)] is observed. With the incident flux as given above, the cross section is 1.06±0.1 mb including correction for undetected decays. The Dalitz plot for this reaction, shown in fig. 1 shows contributions from KΔ(1236), $pK^*(891)$, $pK^*(1420)$ final states. The cross section for these states, as determined from an analysis of both topologies (i) and (ii) are given in table 2. Details of this analysis are given below.

Because of ambiguities in the kinematic fits of the two-prong events, only rough estimates of the $K^+p\pi^o$ and $K^+n\pi^+$ cross sections can be given. If we assign to each of these final states the number of unambiguous fits plus one-half of the ambiguous fits with an error corresponding to one-half the ambiguous fits, we obtain, for the $K^+p\pi^o$ and $K^+n\pi^+$ cross sections, estimates of 0.8±0.2 mb and 0.6±0.3 mb respectively. These estimates are, if anything,

likely to be on the high side since they do not correct for multi-neutral events ambiguous with the one-constraint fits.

3.2. The KΔ(1236) Final State

The data for the study of this state come from topologies (i) and (ii) fitting the reaction (1). To avoid ambiguity problems for the two-prong events we confine ourselves to the region of momentum-transfer-squared between incident and outgoing K, $-t_K < 2\ (GeV/c)^2$. The data from topology (ii) indicates that the Δ population at higher momentum transfers corresponds to a cross section of less than 15 μb, well within the uncertainties of the overall ΔK cross section. In fig. 2 we show the $p\pi^+$ mass distribution for all $K^o p\pi^+$ events of topologies (i) and (ii) with $-t_K < 2\ (GeV/c)^2$ indicating also the ambiguous contribution. It is clear that for $p\pi^+$ masses below 1.8 GeV this contribution is negligible. A fit to the histogram in fig. 1 for $M(p\pi^+) < 1.75$ GeV with a superposition of Δ and phase space leads to a cross section for Δ production in the reaction (1) of 0.42±0.03 mb. The overall KΔ production from K^+p interactions including all final channels is then, using the appropriate Clebsch-Gordan coefficients, 0.56±0.04 mb. The t_K distribution and Δ decay density matrix elements are shown in fig. 3 and fig. 4. The momentum transfer distribution has been fitted to an exponential of the form $(d\sigma/dt) \propto e^{Bt_K}$, $0.2 < -t_K < 1.0\ (GeV/c)^2$, where $B = 4.9 \pm 0.6\ (GeV/c)^{-2}$. Except at very low momentum transfers the density matrix elements are in fairly good agreement with the simple Stodolsky-Sakurai predictions [3] $\rho_{33} = 0.375$, Re $\rho_{3,-1} = 0.21$, Re $\rho_{31} = 0$. This behavior is known to hold over a range of incident momenta from essentially threshold to the highest momenta studied.

The curve shown on fig. 3 is taken from Solution 1 of the Regge-pole model of Krammer and Maor [4] and fits our data reasonably well.

3.3. The $pK^*(891)$ Final State

For momentum-transfer-squared between initial and final proton $-t_p$ less than 1.2 $(GeV/c)^2$ the final proton is recognizable by ionization. With this reaction, one-constraint fits to topology (i) are either unambiguous or have as their only ambiguity an interchange between the outgoing kaon and the outgoing pion. It follows that in this low momentum transfer region the $K^{*+}(891)$ produced in the reaction $K^+ + p \rightarrow p + K^{*+}(891)$ can be detected by plotting the $K\pi$ mass spectrum for all events in the various classes listed in table 3.

For the ambiguous events (last row of table 3) the choice of the $K^o\pi^+$ mass as the one plotted is arbitrary: since the proton is directly recognized and accurately measured, the $K\pi$ mass is essentially independent of whether the $K^o\pi^+p$ or $K^+\pi^op$ fit is the one chosen. The validity of this assertion has been verified experimentally by comparison of $K\pi$ masses in ambiguous events. The mass distribution, for $-t_p < 1.2$ $(GeV/c)^2$, of the events chosen according to table 3 is shown in fig. 5. A large $K^{*+}(891)$ peak is evident and leads to a cross section in this region of momentum transfer of 0.57 ± 0.04 mb for the sum of the $K^o\pi^+$ and $K^+\pi^o$ final states.

For higher momentum transfers, $-t_p > 1.2$ $GeV/c)^2$, the ambiguity problems are somewhat worse in that the proton identification is no longer clear-cut. We show in fig. 6 the $K\pi$ mass spectrum for such events which have at least one fit as $K^op\pi^+$ or $K^+p\pi^o$. Every $K\pi$ mass combination corresponding to an acceptable fit with $-t_p > 1.2$ $(GeV/c)^2$ is shown, except that where $K^op\pi^+$ is ambiguous with $K^+p\pi^o$ with the <u>same</u> particle as proton only the $K^o\pi^+$ mass is shown. The most significant feature in fig. 6 is the large contribution at 1420 MeV which will be discussed in the next section. There is also a small K^* signal near 900 MeV of 12^{+10}_{-5} events, corresponding to a cross section of 10^{+8}_{-4} μb. The overall pK^{*+} cross section for all momentum transfers is then

$0.57 + 0.01 = 0.58 \pm 0.04$ mb. This cross section includes both final states $K^o p\pi^+$ and $K^+ p\pi^o$, and presumably divides itself between them in the ratio 2:1 predicted by Clebsch-Gordan coefficients.

The momentum transfer distribution from the sample of table 3 is shown in fig. 7. It has been fitted to the form

$$\frac{d\sigma}{dt} \propto e^{Bt_p}, \qquad 0.2 < -t_p < 1.0 \ (\mathrm{GeV/c})^2$$

where $B = 3.6 \pm 0.4 \ (\mathrm{GeV/c})^2$. It is perhaps of interest to note that the values of B for both the $K\Delta(1236)$ and the $K^*(891)p$ channels are quite similar to the value $4.2 \pm 0.2 \ (\mathrm{GeV/c})^2$ found in elastic scattering at just the same momentum [2]. It is a priori far from obvious that such a similarity should be expected in view of the importance of Pomeranchuk exchange in the elastic channel and its absence in the channels under discussion.

We now consider the $K^*(891)$ decay, angular distributions and confine ourselves to $-t_p < 1.2 \ (\mathrm{GeV/c})^2$. The events in the last row of table 3 pose a slight problem in that although the $K\pi$ mass and t_p are essentially independent of whether the K^* decay is actually $K^+\pi^o$ or $K^o\pi^+$, the decay angles are sensitive to this choice. A revealing feature of the ambiguity problem is illustrated in fig. 8 which shows the $K^o p\pi^+$ Dalitz plots for two-prong ambiguous and unambiguous events. It is clear from fig. 8 that the low $p\pi^+$ mass half of the $K^*(891)$ band has essentially no ambiguous events. If interference between K^* and either Δ or background is neglected, parity conservation in the K^* decay requires that for every K^* event in the low $p\pi^+$ mass half of the Dalitz plot with Jackson decay angles α, φ there is an event in the high $p\pi^+$ mass half with angles $\pi-\alpha$, $\varphi+\pi$. Consequently events in the unambiguous low $p\pi^+$ mass half of the Dalitz plot give unbiased decay angular distributions provided that appropriate folding is done. This choice of events was thus made for both $K^o p\pi^+$ and $K^+ p\pi^o$ two-prong topologies, retaining of course all K^* events for the unambiguous two-prong-plus-vee topology.

A sample of 350 K^* events so selected gives the density matrix elements shown in fig. 9. The usual pattern of vector exchange dominance ($\rho_{00} \sim 0$) is evident, with significant pion exchange contributions at momentum transfers below 0.1 $(GeV/c)^2$.

3.4. The $pK^*(1420)$ Final State

In figs. 5 and 6 there are substantial enhancements at 1420 MeV for momentum transfers below as well as above 1.2 $(GeV/c)^2$. The enhancements correspond to 80±22 events for $-t_p < 1.2$ $(GeV/c)^2$ and 30±12 events for $-t_p > 1.2$ $(GeV/c)^2$. The corresponding cross sections are 0.065±0.02 mb and 0.025±0.010 mb respectively. Thus the total $K^{*+}(1420)p$ cross section is 0.09±0.025 mb of which 2/3 contributions to the $K^o p\pi^+$ final state and 1/3 to the $K^+ p\pi^o$ final state. It is interesting to note that whereas only about 2% of the $K^*(891)$ events have $-t_p > 1.2$ $(GeV/c)^2$, about 25% of the $K^*(1420)$ are produced with such large momentum transfers.

Because of ambiguities between $K^o\pi^+$ and $K^+\pi^o$ decays of the $K^*(1420)$, limited statistics, and significant background, we have not attempted to study the $K^*(1420)$ decay behavior in this experiment.

4. COMPARISON WITH OTHER EXPERIMENTS

It is of interest to compare the results reported here for K^+p at 4.6 GeV/c with data from K^+p experiments at other momenta done elsewhere and with similar reactions in $\bar{K}N$ experiments. We consider these comparisons in some detail.

4.1. K^+p Experiments at Neighboring Energies

Data on K^* and Δ production in the $K^o p\pi^+$ final state obtained in exposures at 2.97, 3.46, 4.97 and 8.25 GeV/c by the CERN-Brussels Group were presented at the Vienna High Energy Conference [5]. All of our results on cross sections are in reasonable agreement with appropriate interpolations of the CERN-Brussels data.

The slopes B in the differential cross sections $d\sigma/dt \propto e^{Bt_p}$ at 5 GeV/c obtained by the CERN-Brussels group are also in excellent agreement with the values found in the present experiment. It has been pointed out earlier that these slopes agree with the elastic K^+p slope. It is interesting to note that this agreement maintains itself over a large range of momenta, the shrinkage in the elastic data also appearing to about the same extent in the $K^*(891)$ and $\Delta(1236)$ production [5].

The K^* and Δ density matrix elements appear to exhibit momentum transfer dependent behavior which is largely independent of incident momentum. Indeed it has been shown that this momentum independence persists to threshold, a remarkable fact in view of the expectation that on any exchange models, absorptive or Reggeized, the pion exchange contributions to K^* production would be expected to drop much faster as a function of beam energy than do vector exchange contributions [6].

4.2. $\bar{K}N$ Experiments

Two studies of the reaction

$$K^- + p \rightarrow \overline{K^0} + \pi^- + p$$

have been reported for a K^- incident momentum of 4.6 GeV/c [7,8]. The K^{*-} cross sections for this reaction reported are 279±29 μb and 250±20 μb respectively. These values are smaller by a factor of about 1.5 than our measured value of 380±30 μb for reaction (1). At the same time, the K^* density matrix elements reported in both K^-p experiments are in good agreement with the values found in the present experiment over the whole momentum transfer range. This point is illustrated in fig. 9 which shows both our data and the K^-p results of Carmony et al. [8].

If one attempts to describe the reactions $K^+p \rightarrow K^{*+}p$ and $K^-p \rightarrow K^{*-}p$ in terms of a Regge pole model with exchange-degenerate P'-ω exchange, the K^+

and the K^- processes should have the same cross section and the same density matrix elements. The simultaneous presence of some ρ-A_2 exchange would be expected to have little effect on this expectation since the ρ-A_2 trajectory is practically the same as the P'-ω trajectory. Furthermore π or exchange-degenerate π-B exchange, in the absence of interference with the vector-tensor exchanges, would also leave the prediction unaffected. As indicated above, the simple prediction is satisfied for the density matrix elements but fails by about a factor of 1.5 for the absolute cross sections.

At lower energies, the work of Donohue [9], based principally on data from Friedman and Ross [10], suggests a difference between K^{*-} and K^{*+} production in both the shape of $\frac{d\sigma}{dt}$ and the value of ρ_{00} near the forward direction. It appears that for K^{*-}, both $\frac{d\sigma}{dt}$ and ρ_{00} rise much more sharply at small t than for K^{*+}; Donohue has interpreted this behavior in terms of constructive interference between π and ω exchange in K^{*-} and destructive interference in K^{*+}. There is no evidence for such a difference in the shape of $\frac{d\sigma}{dt}$ and ρ_{00} in the 4.6-GeV data.

It is interesting to note that a recent study of Brody et al. [11] of the reactions $K^0p \to K^{*0}p$ and $\overline{K^0} \to \overline{K^{*0}}p$ yields nearly equal cross sections for these reactions over momenta from 2 to 7 GeV/c. This observation is completely compatible with our comparison of $K^+p \to K^{*+}p$, $K^-p \to K^{*-}p$ and the following features of the reactions $K^+n \to K^{*+}n$, $K^-n \to K^{*-}n$ which are charge symmetric counterparts of the reaction discussed by Brody et al.: (a) The cross section for $K^+n \to K^{*+}n$ appears to be about a factor of 1.5 to 2 lower than that for $K^+p \to K^{*+}p$ [12]; (b) the cross section for $K^-n \to K^{*-}n$ seems to be nearly equal to that for $K^-p \to K^{*-}p$ [8]. Thus the cross section for $K^-n \to K^{*-}n$ would be expected to be about equal to that for $K^+n \to K^{*+}n$ in good agreement with the observations of Brody et al. for the charge symmetric reactions.

An even more interesting comparison is that between our $K^+p \to K^o\Delta^{++}$ and the reaction $K^-n \to \overline{K^o}\Delta^-$ also studied by Carmony et al. [8] where only the ρ-A_2 exchange combination is expected to be important. Again, with greater force because of the small number of expected exchanges, one predicts on the basis of exchange degeneracy equality of cross sections and density matrix elements. As fig. 4 shows, within rather poor statistics, the equality of matrix elements is indeed fulfilled. However, the K^- cross section of 162±12 μb is far below our value of 420±30 μb for the K^+ cross section. This large difference is all the more surprising because, as pointed out by Cline et al. [13] at 5.5 GeV/c and Firestone et al. [14] at 12 GeV/c the K^+ and K^- elastic charge exchange processes, which involve precisely the same t-channel exchanges as the KΔ production, have virtually equal cross sections and t distributions, and furthermore the t distributions of the elastic charge exchange processes have essentially the same shape as for the KΔ final states.

This deviation from the prediction of ρ-A_2 degeneracy has already been pointed out by Lai and Louie [15]. Indeed fig. 4 of their paper suggests that unlike elastic charge exchange, in which discrepancies exist at low momenta but disappear at 5 GeV/c, the cross-section difference between KΔ production by K^+ and K^- does not seem to disappear at high momenta, although a conclusive test will require data for the K^-n reaction at higher momenta than presently available. The recent results of Brody et al. [11] also indicate a low cross section for the reaction $\overline{K^o}p \to K^-\Delta^{++}$ relative to $K^+p \to K^o\Delta^{++}$ over the momentum range from 2 to 7 GeV/c.

It is worth noting that the inequality of the cross sections for ΔK production in KN and $\overline{K}N$ reactions considerably improves agreement between experiment and the SU(3) prediction, applicable in the t-channel exchange domain:

$$\frac{1}{2}\left[\frac{d\sigma}{dt}(K^+p \to K^o\Delta^{++}) + \frac{d\sigma}{dt}(K^-n \to \overline{K^o}\Delta^-)\right] = \frac{1}{2}\left[\frac{d\sigma}{dt}(\pi^+p \to \pi^o\Delta^{++})\right] + \frac{3}{2}\left[\frac{d\sigma}{dt}(\pi^+p \to \eta\Delta^{++})\right] . \quad (5)$$

Mathews [16] tested this prediction assuming exchange degeneracy to replace the left side of the equation by $\frac{d\sigma}{dt}(K^+p \to K^o\Delta^{++})$. His results indicate that the left side, after the above replacement, is about 20% higher than the right side over the t range up to $-t = 0.8$ $(GeV/c)^2$. With the correct form of eq. (5), the inequality of the K and $\overline{K}$ cross sections brings improved agreement between theory and experiment.

We conclude this discussion by showing in fig. 10 comparisons of $d\sigma/dt$ distributions for the following reaction pairs: (a) elastic K^+p [2] and K^-p [17] at 4.6 GeV/c, (b) charge exchange $K^+n \to K^op$ and $K^-p \to \overline{K^o}n$ at 5.5 GeV/c [13], (c) $K^+p \to K^{*+}p \to K^o\pi^+p$ and $K^-p \to K^{*-}p \to \overline{K^o}\pi^-p$ at 4.6 GeV/c [8], and (d) $K^+p \to K^o\Delta^{++} \to K^op\pi^+$ and $K^-n \to \overline{K^o}\Delta^- \to \overline{K^o}n\pi^-$ [8] at 4.6 GeV/c. The curves shown are approximate representations of the experimental data rather than fits and are not to be taken too literally. All logarithmic slopes are nearly the same, namely about 4 $(GeV/c)^{-2}$ with the exception of K^-p elastic scattering whose slope is about 7 $(GeV/c)^{-2}$. Indeed both in the shape of $d\sigma/dt$ and in the final state alignments K^+ and K^- nonelastic two-body final states related through $s \longleftrightarrow u$ crossing are very similarly behaved. The cross sections however differ substantially in some of the processes. It is hard to see how these differences are easily interpretable in terms of absorption effects; such effects would generally lead to changes in density matrix elements and modifications of the shape of $d\sigma/dt$ which are not observed.

We express our appreciation to Gerson Goldhaber for a useful discussion, to our scanning and measuring and programming staff, to the FSD operating staff under Howard White, and to the BNL 80-inch bubble chamber crew.

REFERENCES

[1] C. Fu, Lawrence Radiation Laboratory Report UCRL-18417 (1968), unpublished.

[2] J. N. MacNaughton, L. Feinstein, F. Marcelja, and G. H. Trilling, Nucl. Phys. B14 (1969) 237.

[3] L. Stodolsky and J. J. Sakurai, Phys. Rev. Letters 11 (1963) 90.

[4] M. Krammer and U. Maor, Nucl. Phys. B13 (1969) 651.

[5] W. De Baere et al., Paper submitted to the XIVth International Conference on High-Energy Physics, Vienna (1968).

[6] R. W. Bland et al., Nucl. Phys. B18 (1970) 537.

[7] Y. W. Kang, Phys. Rev. 176 (1968) 1587.

[8] D. D. Carmony, H. W. Clapp, A. F. Garfinkel, L. J. Gutay, D. H. Miller, and R. L. Eisner, Nucl. Phys. B12 (1969) 9; D. D. Carmony, R. L. Eisner, A. C. Ammann, A. F. Garfinkel, L. J. Gutay, D. H. Miller, L. K. Rangan, and W. L. Yen, Preprint COO-1428-166 (1970), Purdue University.

[9] J. T. Donohue, Phys. Rev. 163 (1967) 1549.

[10] J. H. Friedman and R. R. Ross, Phys. Rev. Letters 16 (1966) 485, 832(E).

[11] A. D. Brody et al., SLAC Preprint (1970).

[12] G. Bassompierre et al., Nucl. Phys. B16 (1970) 125; A. A. Hirata, private communication (1970).

[13] D. Cline, J. Matos, and D. D. Reeder, Phys. Rev. Letters 23 (1969) 1318.

[14] A. Firestone, G. Goldhaber, A. Hirata, D. Lissauer, and G. H. Trilling, Phys. Rev. Letters 25 (1970) 958.

[15] K. W. Lai and J. Louie, Nucl. Phys. B19 (1970) 205.

[16] R. Mathews, Nucl. Phys. B11 (1969) 339.

[17] L. S. Schroeder, R. A. Leacock, R. L. Wagstaff, and W. J. Kernan, Phys. Rev. 176 (1968) 1648.

Table 1. Numbers of fits in the various channels.

	Unambiguous	Ambiguous
$K^+p\pi^o$	666	501
$K^op\pi^+$ (with K^o decay)	482	0
$K^op\pi^+$ (without K^o decay)	931	591
$K^+\pi^+n$	434	700

Table 2. Cross sections for various single pion final states produced.

Final state	Contribution to $K^op\pi^+$	Total one-pion contribution
$K\Delta$	0.42±0.03 mb	0.56±0.04 mb
$K^*(891)p$	0.38±0.03 mb	0.58±0.04 mb
$K^*(1420)p$	0.06±0.02 mb	0.09±0.03 mb
All other states	0.20±0.11 mb	~ 1.3 mb

Table 3. Classes of events used in study of pK^* final state.

Topology	Reaction	Fit used
(ii)	Unambiguous $K^op\pi^+$	$K^op\pi^+$
(i)	Unambiguous $K^op\pi^+$	$K^op\pi^+$
(i)	Unambiguous $K^+p\pi^o$	$K^+p\pi^o$
(i)	Ambiguous $K^op\pi^+$ or $K^+p\pi^o$	$K^op\pi^+$

FIGURE CAPTIONS

Fig. 1. Dalitz plot for the $K^o p\pi^+$ final state including only events with a visible K^o decay.

Fig. 2. $p\pi^+$ mass spectrum in the $K^o p\pi^+$ final state with $-t_K < 2$ (GeV/c)^2. All topologies are included, and ambiguous events are shaded.

Fig. 3. Momentum transfer distribution in the reaction $K^+p \rightarrow K^o\Delta^{++} \rightarrow K^o p\pi^+$. The curve is from the fit given by Krammer and Maor [4].

Fig. 4. Density matrix elements for the Δ from the reaction $K^+p \rightarrow K^o\Delta^{++}$, shown as solid crosses. Dashed crosses are from the reaction $K^-n \rightarrow \overline{K^o}\Delta^-$ at essentially the same momentum, from the paper of Carmony et al. [8].

Fig. 5. $K\pi$ mass spectrum for the event classes chosen as in table 3, with $-t_p < 1.2$ (GeV/c)^2 and removal of events in the Δ^{++} band.

Fig. 6. $K\pi$ mass spectrum for $-t_p > 1.2$ (GeV/c)^2. Events in the Δ^{++} band have been removed and ambiguities treated as discussed in the text.

Fig. 7. Momentum transfer distribution in the reaction $K^+p \rightarrow K^{*+}(891)p \rightarrow K^o\pi^+p$. Events have been selected just as for fig. 5, and normalized to the cross section of 0.38 mb for the $K^o\pi^+p$ final state.

Fig. 8. Dalitz plots for ambiguous and unambiguous fits to the $K^o p\pi^+$ state. Only the two-prong events are plotted.

Fig. 9. Density matrix elements for the $K^*(891)$ from the reaction $K^+p \rightarrow K^{*+}p$. Dashed crosses are from the reaction $K^-p \rightarrow K^{*-}p$ at the same momentum from the paper of Carmony et al. [8].

Fig. 10. Comparison of $d\sigma/dt$ for various final states produced by K^+N and K^-N interactions. Solid lines represent K^+N, and dashed lines K^-N processes.

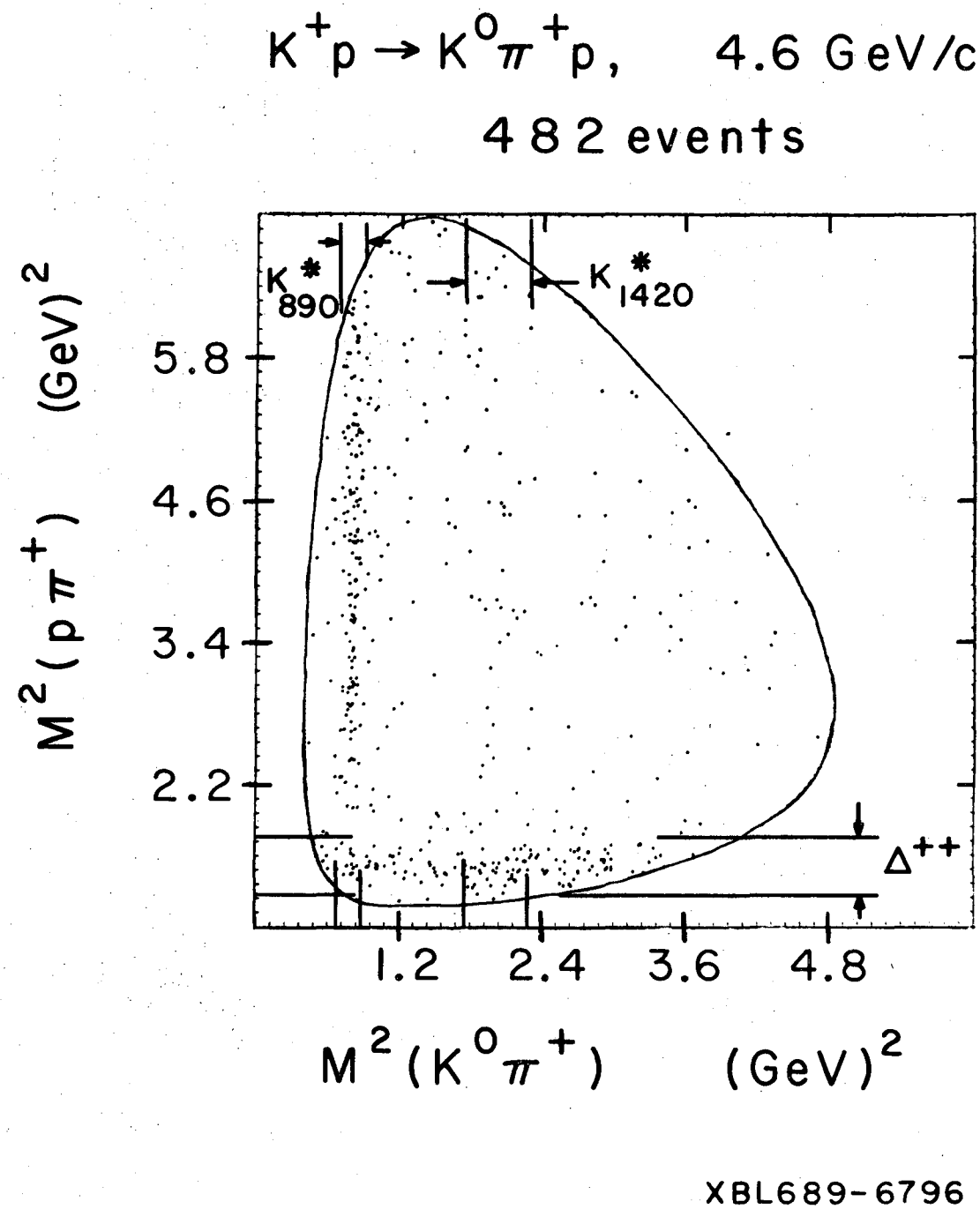
$K^+p \rightarrow K^0\pi^+p$, 4.6 GeV/c
482 events
K^*_{890}
K^*_{1420}
Δ^{++}
5.8
4.6
3.4
2.2
1.2
2.4
3.6
4.8
$M^2(p\pi^+)$ (GeV)^2
$M^2(K^0\pi^+)$ (GeV)^2
XBL689-6796

Fig. 1

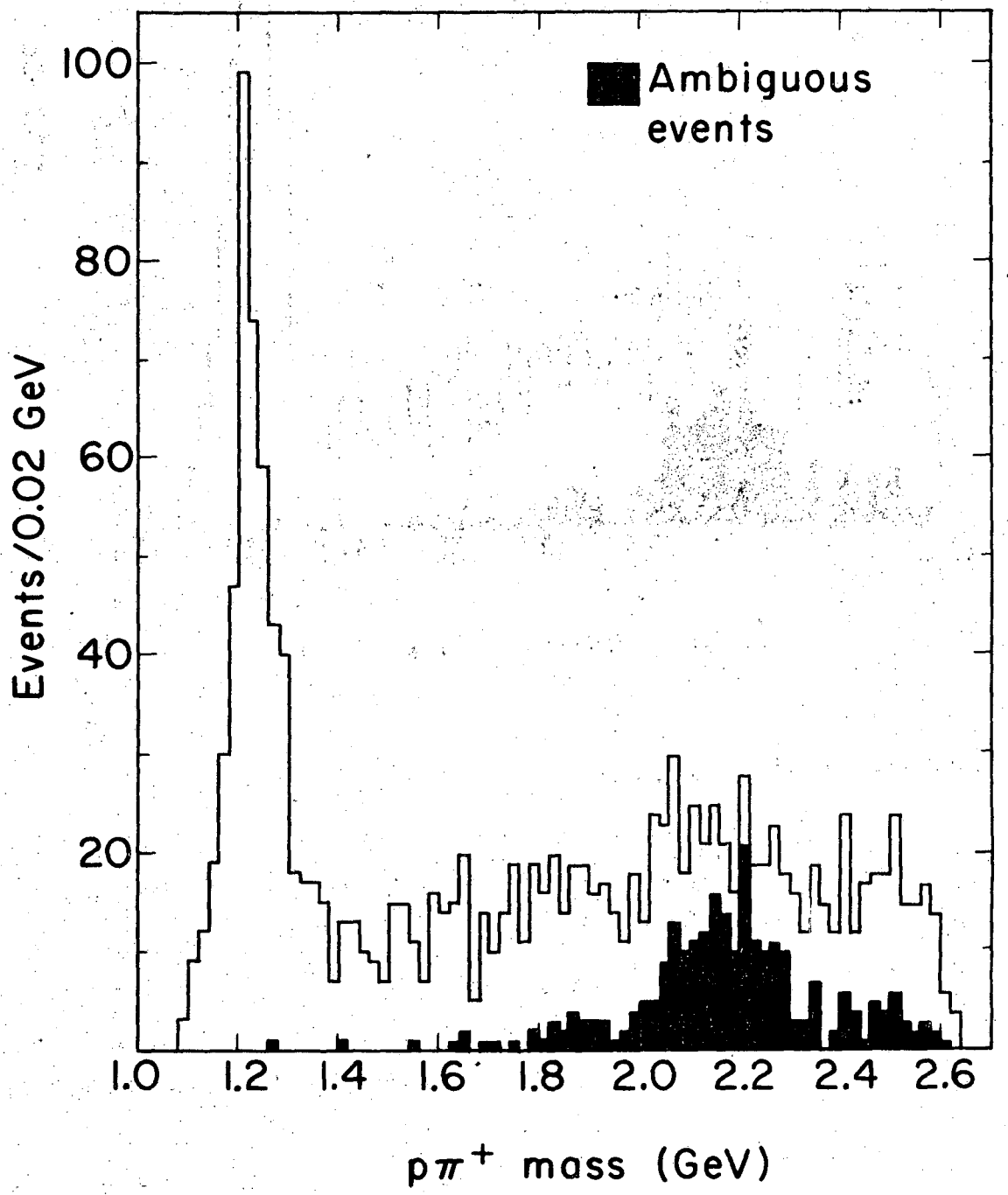

XBL706-3146

Fig. 2

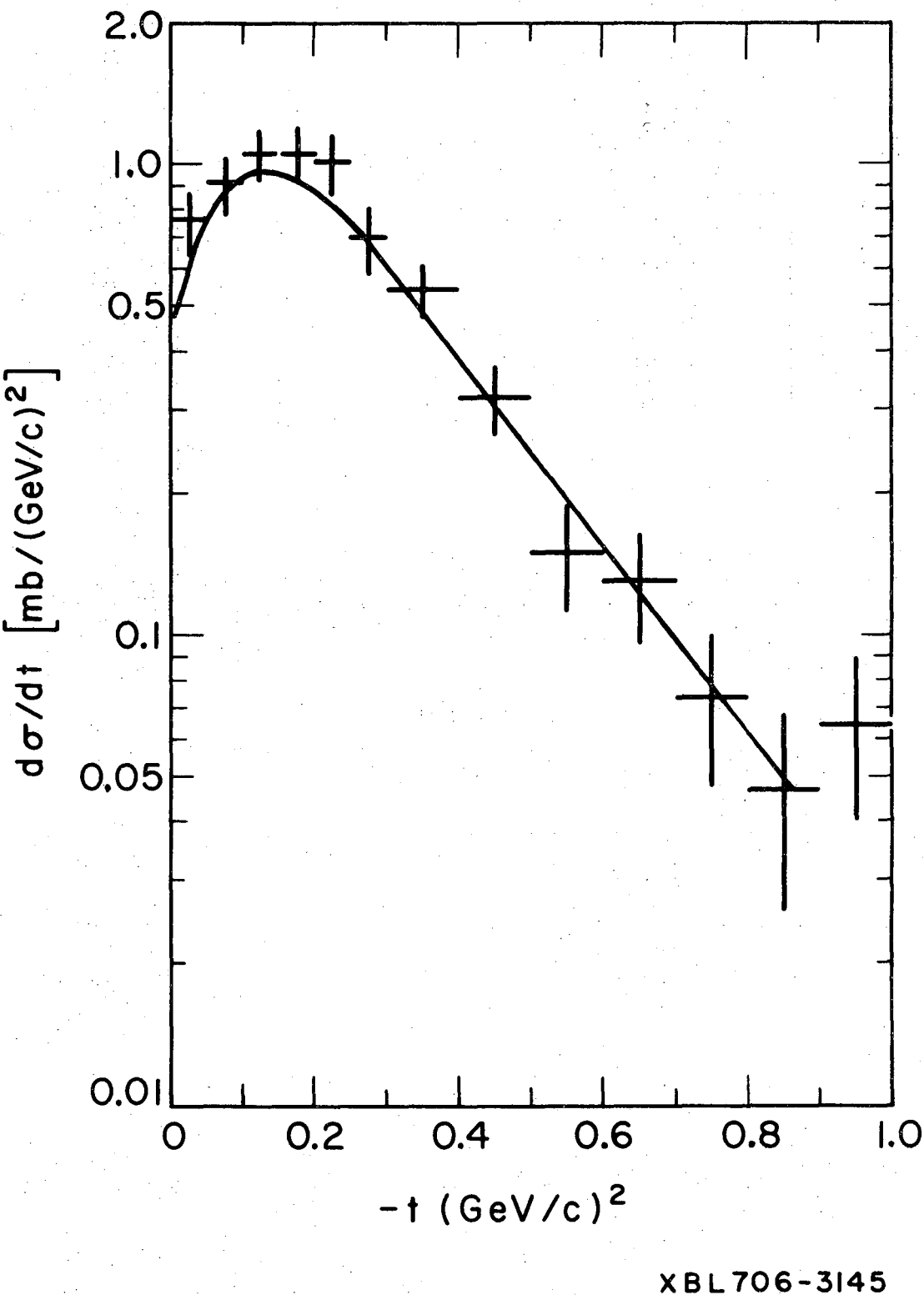
2.0
1.0
0.5
0.1
0.05
0.01
dσ/dt [mb/(GeV/c)²]
0
0.2
0.4
0.6
0.8
1.0
-t (GeV/c)²
XBL706-3145

Fig. 3

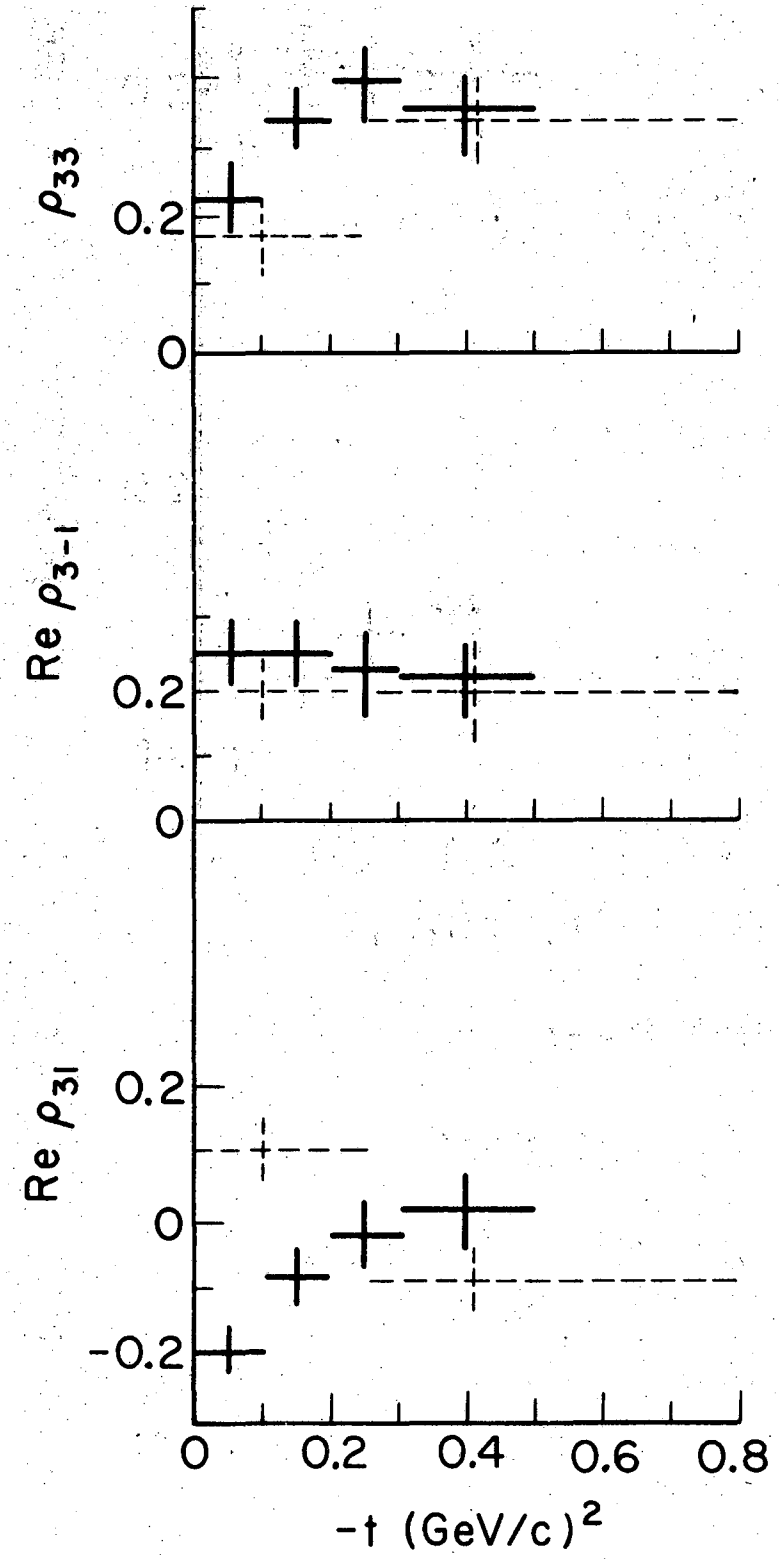

XBL-706-3144

Fig. 4

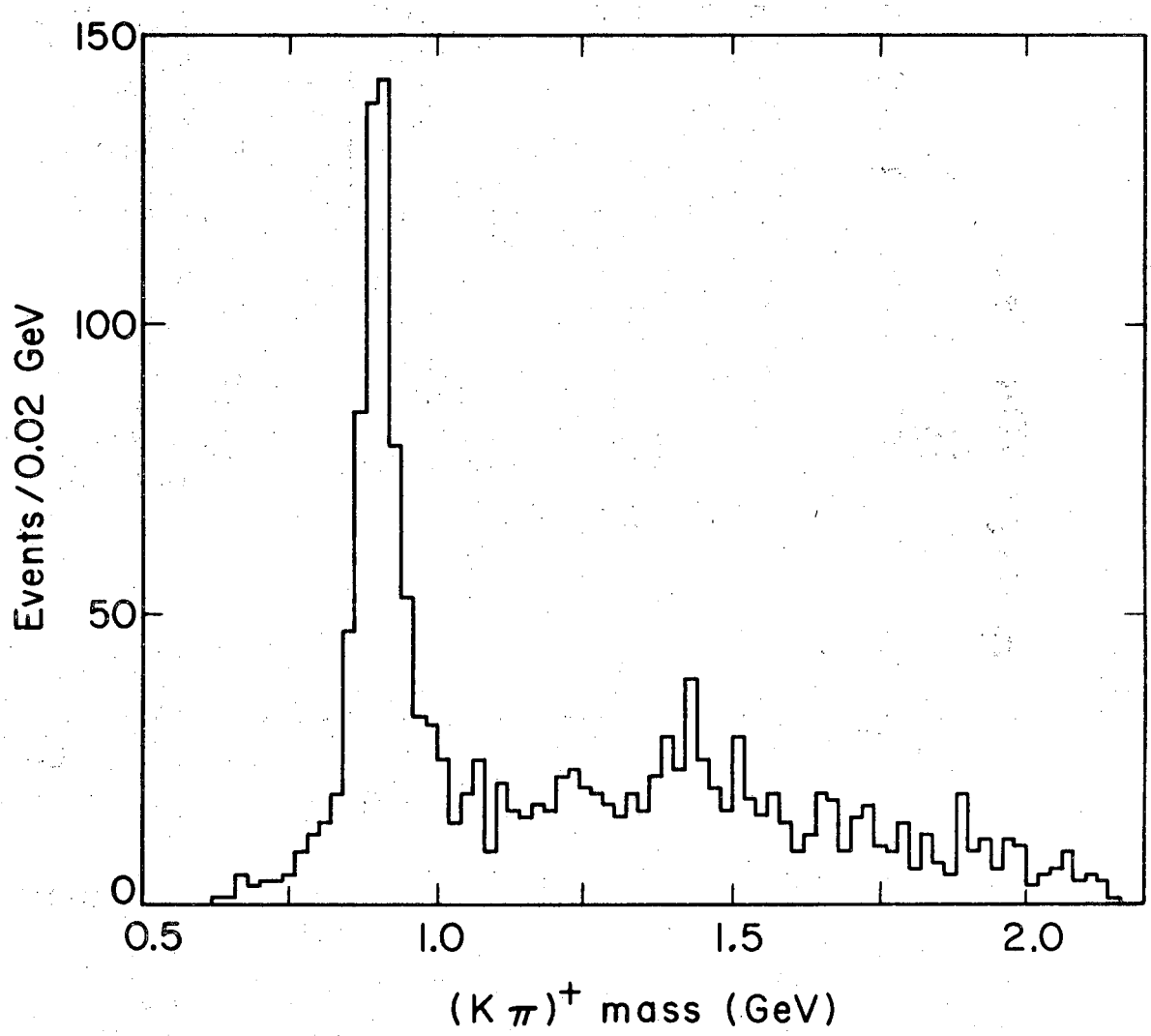

XBL706-3143

Fig. 5

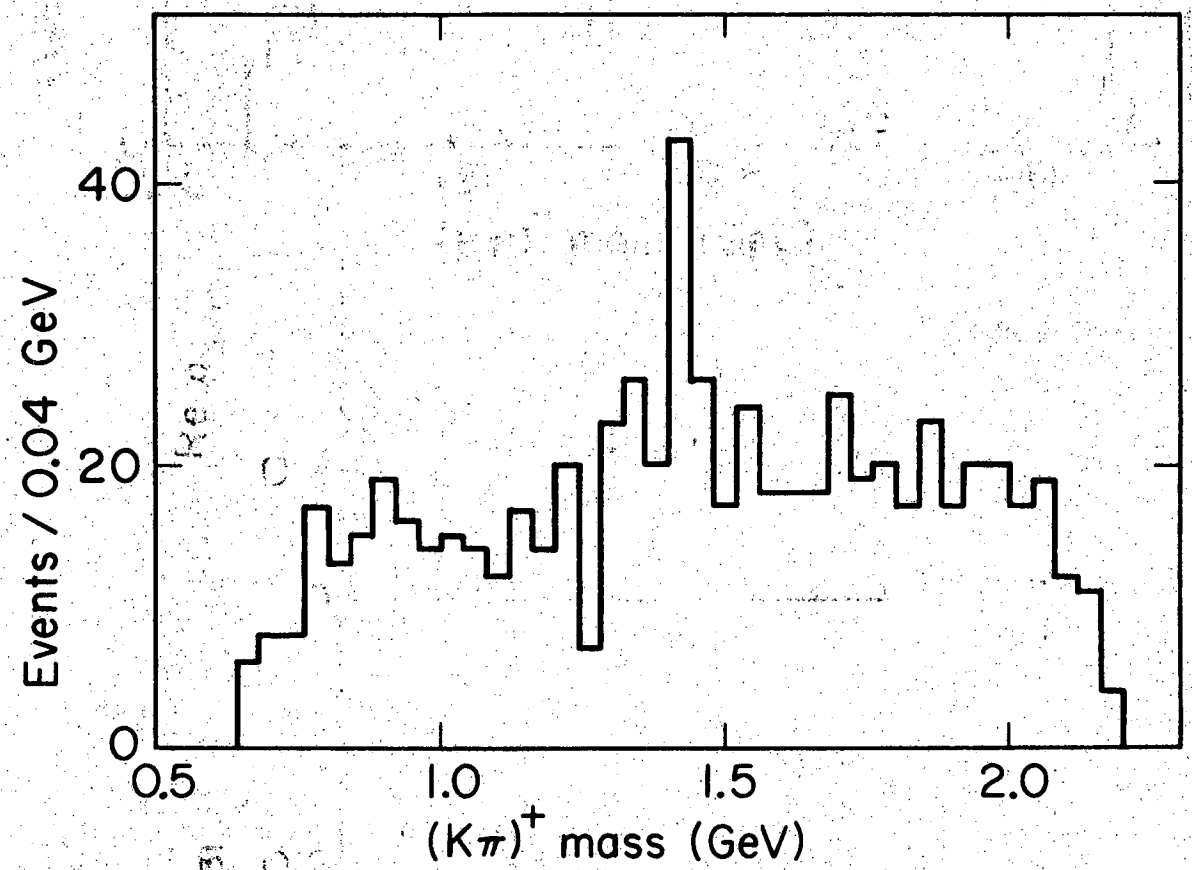

XBL709-3788

Fig. 6

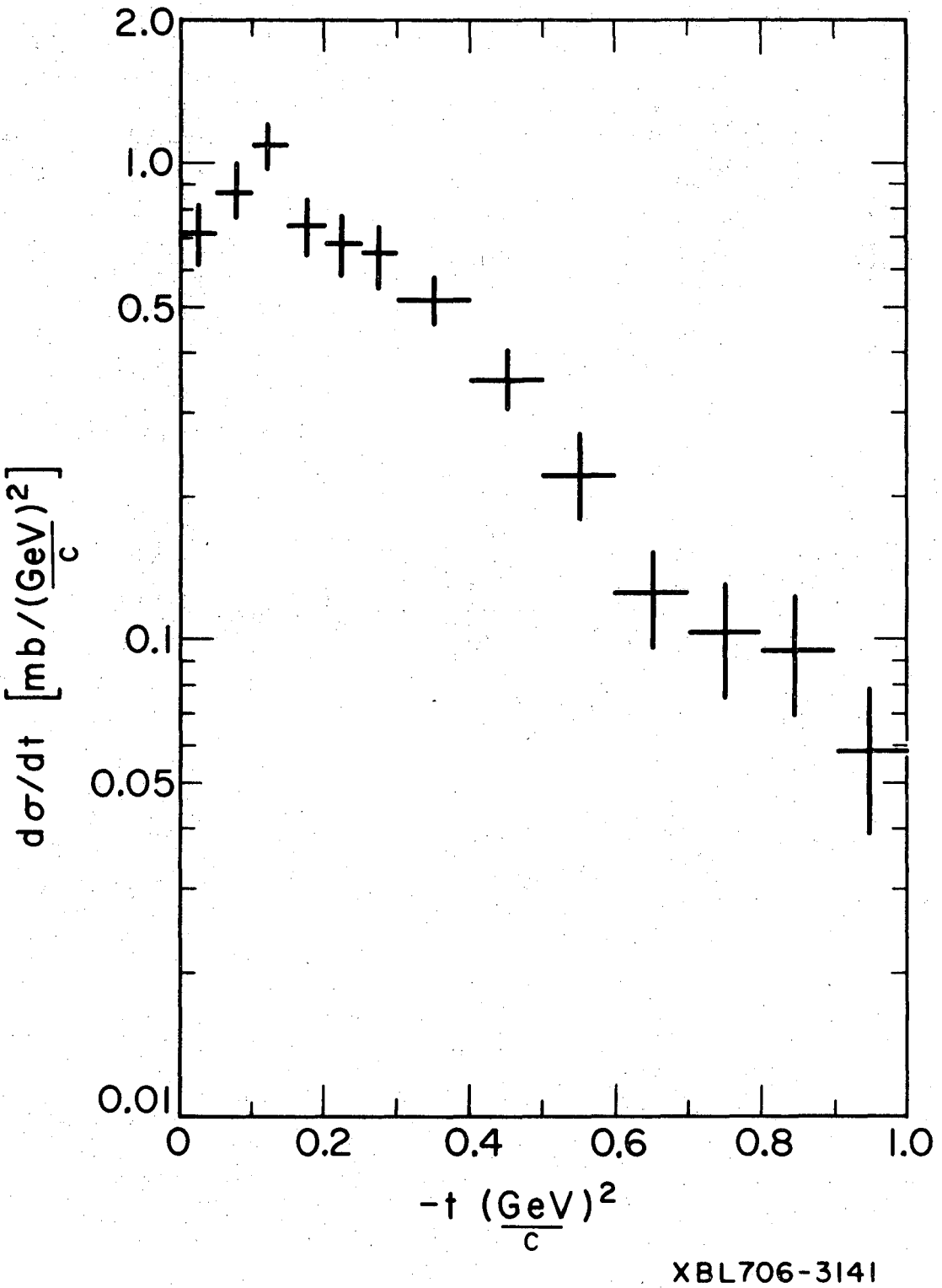
2.0
1.0
0.5
0.1
0.05
0.01
0
0.2
0.4
0.6
0.8
1.0
dσ/dt [mb/(GeV/c)²]
-t (GeV/c)²
XBL706-3141

Fig. 7

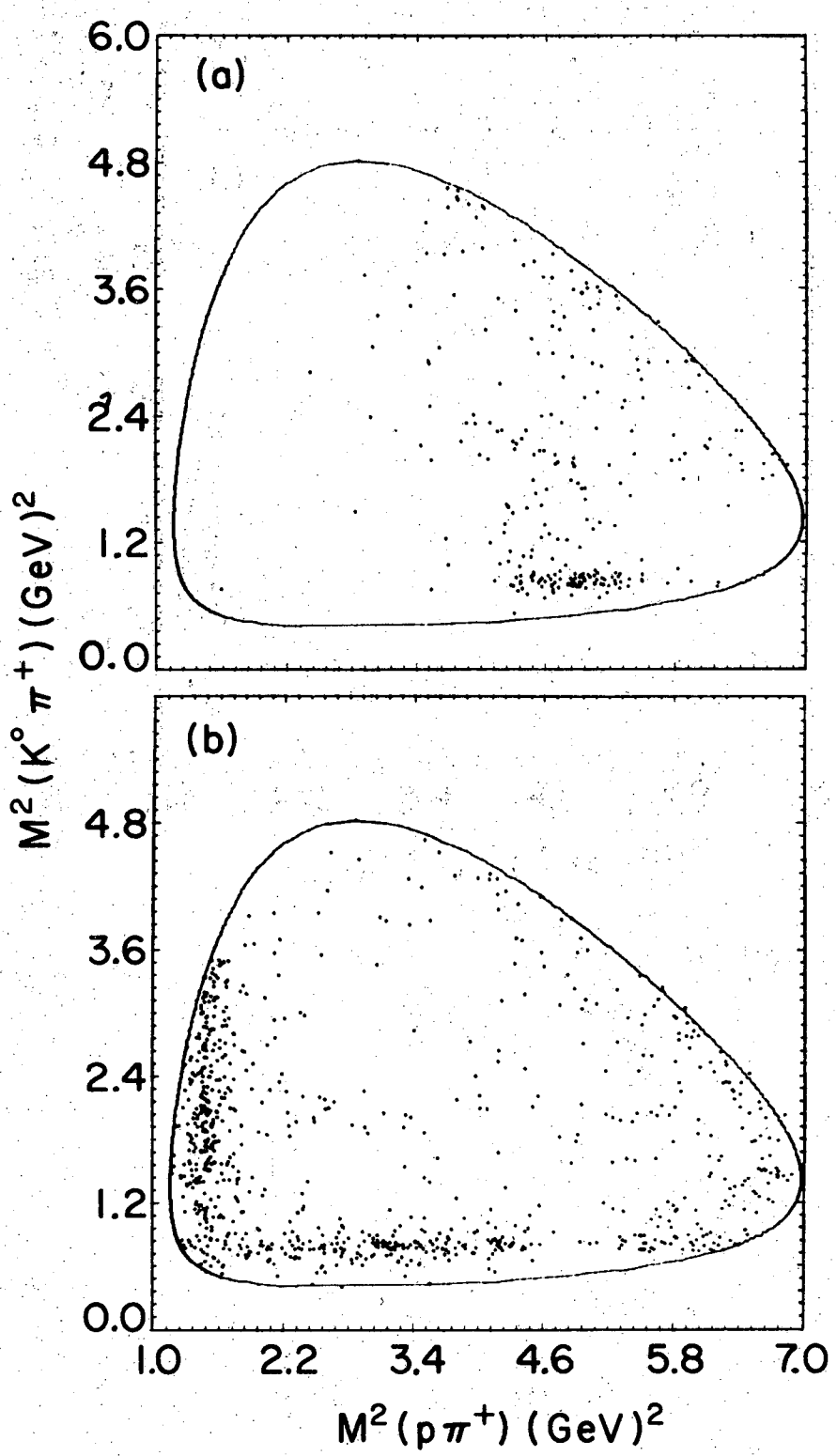

XBL706-3140

Fig. 8

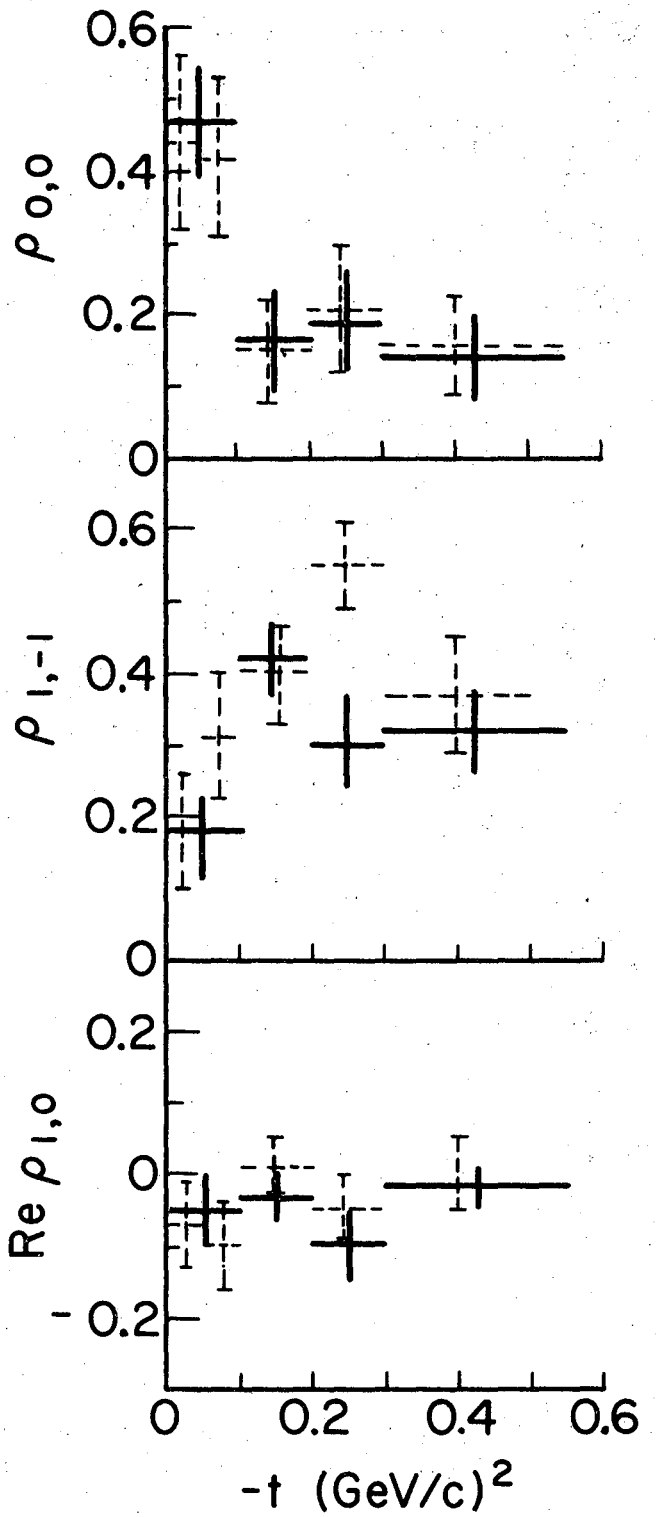

XBL706-3188

Fig. 9

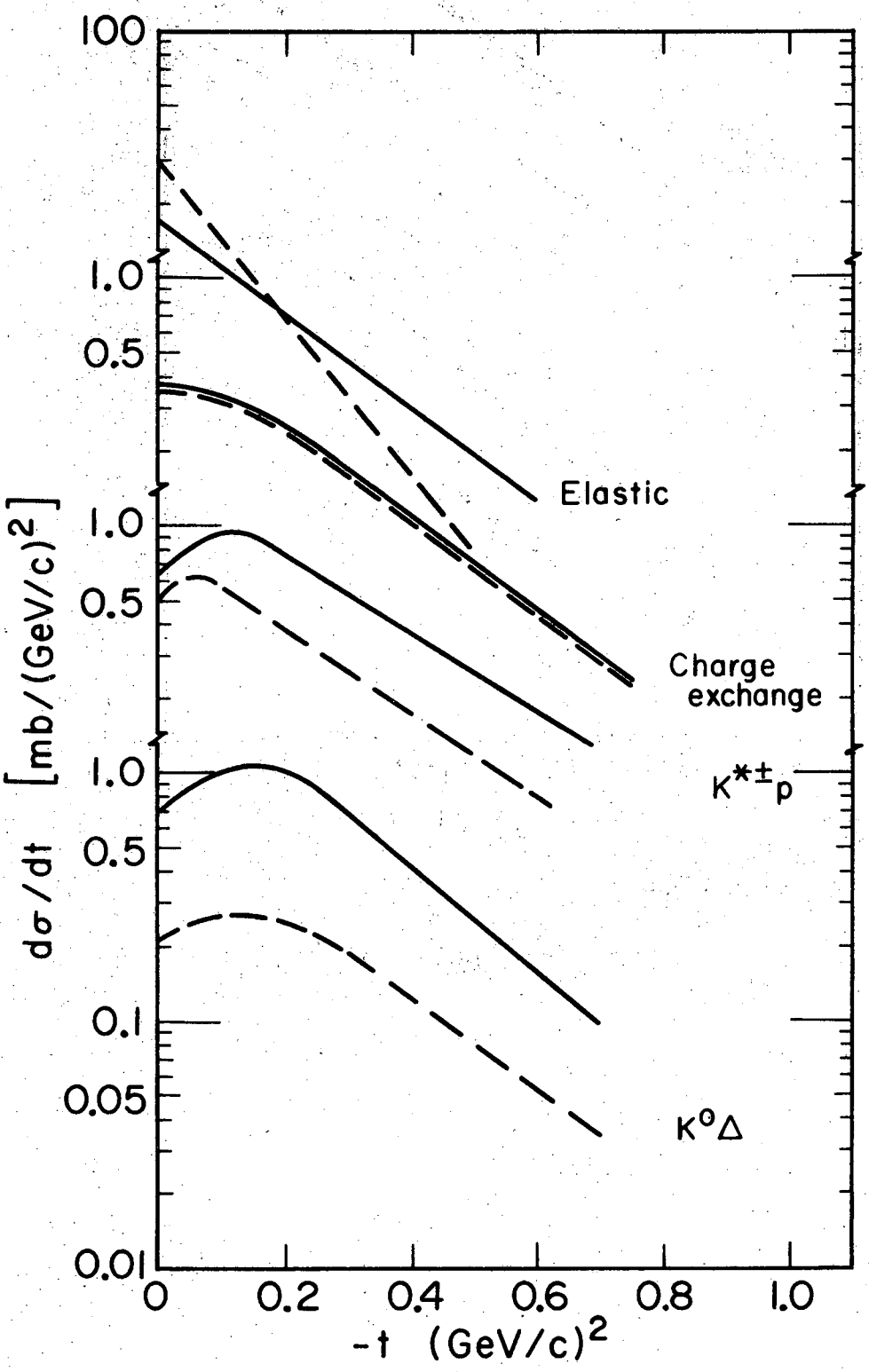
100
1.0
0.5
1.0
0.5
1.0
0.5
0.1
0.05
0.01
dσ/dt [mb/(GeV/c)²]
Elastic
Charge exchange
K*±p
K⁰Δ
0
0.2
0.4
0.6
0.8
1.0
-t (GeV/c)²
XBL709-3789

Fig. 10